

Theta–gamma coordination between anterior cingulate and prefrontal cortex indexes correct attention shifts

Benjamin Voloh^a, Taufik A. Valiante^{b,c}, Stefan Everling^d, and Thilo Womelsdorf^{a,d,1}

^aDepartment of Biology, Centre for Vision Research, York University, Toronto, ON M6J 1P3, Canada; ^bDivision of Fundamental Neurobiology, Toronto Western Research Institute, Toronto, ON M5T 2S8, Canada; ^cDivision of Neurosurgery, Department of Surgery, University of Toronto, Toronto, ON M5T 1P5, Canada; and ^dDepartment of Physiology and Pharmacology, Centre for Functional and Metabolic Mapping, University of Western Ontario, London, ON N6A 5B7, Canada

Edited by Robert Desimone, Massachusetts Institute of Technology, Cambridge, MA, and approved May 26, 2015 (received for review January 10, 2015)

Anterior cingulate and lateral prefrontal cortex (ACC/PFC) are believed to coordinate activity to flexibly prioritize the processing of goal-relevant over irrelevant information. This between-area coordination may be realized by common low-frequency excitability changes synchronizing segregated high-frequency activations. We tested this coordination hypothesis by recording in macaque ACC/PFC during the covert utilization of attention cues. We found robust increases of 5–10 Hz (theta) to 35–55 Hz (gamma) phase-amplitude correlation between ACC and PFC during successful attention shifts but not before errors. Cortical sites providing theta phases (i) showed a prominent cue-induced phase reset, (ii) were more likely in ACC than PFC, and (iii) hosted neurons with burst firing events that synchronized to distant gamma activity. These findings suggest that interareal theta–gamma correlations could follow mechanistically from a cue-triggered reactivation of rule memory that synchronizes theta across ACC/PFC.

attention | prefrontal cortex | anterior cingulate cortex | theta oscillation | gamma oscillation

The anterior cingulate and prefrontal cortex (ACC/PFC) of primates are key structures that ensure the flexible deployment of attention during goal-directed behavior (1, 2). To achieve such flexible control, diverse streams of information need to be taken into account, which are encoded by neuronal populations in anatomically segregated subfields of the ACC/PFC (3, 4). Information about the expected values of possible attentional targets are prominently encoded in medial prefrontal cortices and ACC, whereas the rules and task goals that structure goal-directed behavior are prominently encoded in the lateral PFC (5, 6). Flexible biasing of attention thus requires the integration of information across anatomically segregated cortical circuits. One candidate means to achieve such interareal integration is by synchronizing local processes in distant brain areas to a common process. A rich set of predominantly rodent studies have documented such interareal neuronal interactions in the form of a phase–amplitude (P–A) correlations between low-frequency periodic excitability fluctuation and high-frequency gamma-band activity (7–9). It is, however, unknown whether there are reliable cross-frequency P–A interactions between those primate ACC/PFC nodes that underlie flexible attention shifts and, if so, whether P–A correlations are reliably linked to the actual successful deployment of attention (10, 11). We thus set out to test for and characterize P–A interactions during covert control processes by recording local field potential (LFP) activity in macaque ACC/PFC subfields during attentional stimulus selection.

Results

We recorded LFP activity from 1,104 between-channel pairs of electrodes (344 individual LFP channels) within different subfields in ACC/PFC of two macaques engaged in an attention task (Fig. 1A). In the following, we report results pooled across monkeys and show that individual monkey results were consistent and qualitatively similar in *SI Result S1*. These recordings were from a dataset that was previously analyzed with respect to neuronal

firing and burst–LFP synchronization (3, 12, 13) (*SI Methods*). During each trial, covert spatial attention had to be shifted toward one of two peripheral stimuli in response to the color of a centrally presented cue stimulus (Fig. 1A). Covert spatial attention then had to be sustained on the target stimulus until it transiently rotated clockwise or counterclockwise. The animals obtained fluid reward when they correctly discriminated the rotation of the attended stimulus. On one-half of the trials, the distracting non-target stimulus rotated before the target stimulus. Both monkeys successfully ignored this distractor change, indicating correct attentional deployment on the target with an average accuracy of $82.6 \pm 0.7\%$ SE and errors committed in response to the distractor rotation in $4.5 \pm 0.2\%$ SE) (*SI Result S2*).

Attention Cue Triggers Theta–Gamma P–A Correlations. In the outlined task, attention shifts required the use of task knowledge to successfully combine color and location information to prioritize the correct stimulus. ACC/PFC subfields are core circuits supporting the flexible integration of information to shift attention (2, 3). To test whether the attention shift is accompanied by cross-frequency interactions, we selected LFP pairs recorded from different sites in ACC and PFC (Fig. 1B and Figs. S1 and S2) and quantified how high-frequency activity variations related to the phases of slow frequency activity modulation around the time of the attention cue. In multiple-example LFP pairs, we observed that the attention cue onset triggered sequences of brief bursts of gamma-band activity that synchronized to a narrow phase range of periodic 5- to 10-Hz theta-band activity recorded at distant sites (Fig. 1C and Fig. S2). To quantify whether these cross-frequency correlations were reliably linked to attention shifts, we calculated

Significance

During flexible goal-directed behavior, our frontal cortex coordinates goal-relevant information from widely distributed neuronal systems to prioritize the relevant over irrelevant information. This coordination may be realized by entraining multiple distributed systems with slow activity oscillation to phase-align their local fast oscillatory activity. We analyzed this spatially distributed oscillatory coupling in macaques during actual attentional stimulus selection. We identified that successful—but not failed—selection of relevant information followed the coupling of slow and fast frequencies at narrow oscillation phases, with interareal anatomical specificity, and based on a reset mechanism for the slow oscillation. These findings suggest a specific functional and mechanistic solution to the fundamental coordination problem in primate brains.

Author contributions: T.W. designed research; S.E. and T.W. performed research; B.V., T.A.V., and T.W. contributed new reagents/analytic tools; B.V. and T.W. analyzed data; and B.V. and T.W. wrote the paper.

The authors declare no conflict of interest.

This article is a PNAS Direct Submission.

¹To whom correspondence should be addressed. Email: thiwom@yorku.ca.

This article contains supporting information online at www.pnas.org/lookup/suppl/doi:10.1073/pnas.1500438112/-DCSupplemental.

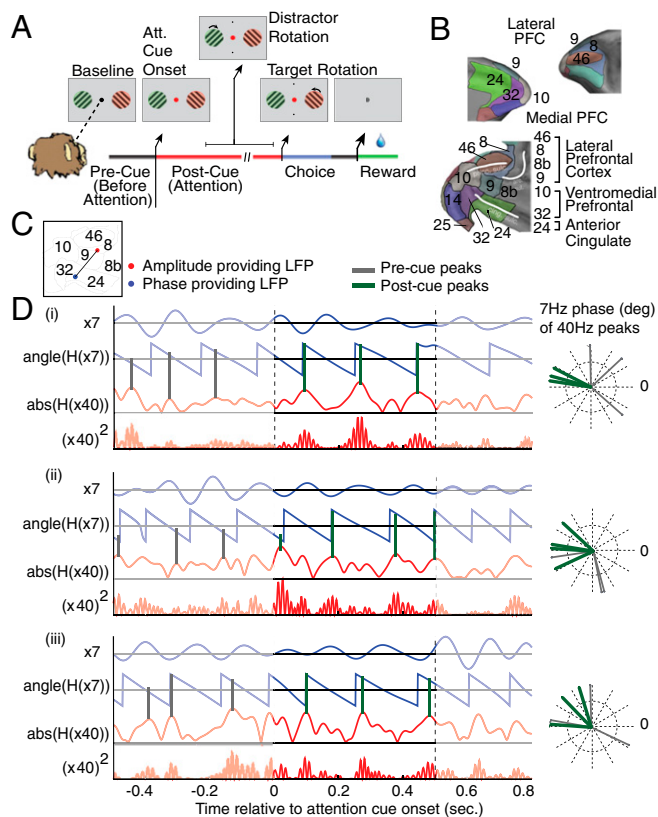


Fig. 1. Task and illustration of example theta-gamma correlation. (A) The selective attention task required monkeys to keep fixation on a central cue throughout a trial, while presented with two peripheral grating stimuli. First, both grating stimuli changed their color simultaneously to either green or red, the location of which was random. Then, the fixation point changed its color to match the stimulus to which the monkey has to covertly shift attention. The attended stimulus rotated transiently at unpredictable times, requiring the monkey to judge a clockwise/counterclockwise rotation to receive fluid reward. Rotations of the nonattended stimulus had to be ignored (filtered). (B) Lateral and medial prefrontal cortex of macaques rendered in 3D (upper panels) and represented as 2D flat map (bottom panel) with a standard labeling of cortical fields (for details, see Fig. S1). Adapted from ref. 3. (C) Anatomical locations on the 2D flat map of an example LFP pair in which the LFP theta phase of one recording site in the ACC (blue dot) correlated with the low-gamma amplitude of a second LFP recording site in LFP area 8 (red dot). (D) Filtered phase and amplitude traces for the example LFP-LFP pair that is shown in C for three trials (*i-iii*). For each trial, the bandpass-filtered low-frequency activation and its phase evolution are shown with blue lines, and the amplitude envelope and the squared gamma amplitude of the amplitude-providing LFP recording are shown in red. Gray (green) vertical lines highlight the phases at which the gamma-amplitude variations show peaks within the 500 ms before (after) attention cue onset. The polar plot on the *Right* shows these peak phases in the precue and postcue epoch. For this ACC-LPFC example pair, the gamma-amplitude peaks of the PFC channel correlate with similar theta phases of the ACC channel in the postcue period. For more examples, see Fig. S2.

the change in Tort's modulation index (MI) (14) in 0.5-s time windows following the attention cue vs. before the cue. Across all between-channel LFP pairs, we found a significant increase in cross-frequency correlations between the phase of a ~ 7 -Hz theta frequency, and the amplitude of ~ 40 -Hz gamma-frequency activity [Wilcoxon sign-rank test, $P = 1.6 \times 10^{-4}$, false discovery rate (FDR) corrected; Fig. 2*A* and *B* and Fig. S3]. Across all LFP pairs, the theta-gamma P-A correlations increased on average by $61.73 \pm 0.037\%$ SE (average normalized change in MI: 0.0556 ± 0.0109 SE; Fig. 2*B*). For the 7- to 40-Hz theta-gamma frequency combination that showed maximal correlation, $n = 85$ LFP pairs (85 of 1,104; 7.7%) showed a statistically significant increase in

P-A correlation following the attention cue (Monte Carlo surrogate test, at least $P < 0.05$; Fig. 2*B*). In the following, we characterize these 85 LFP pairs that showed an increased theta-gamma correlation in the postcue period that was also evident in the average across the population of LFP pairs [see *SI Result S3* for a characterization of $n = 46$ (4.2%) LFP pairs showing significant reductions in theta-gamma correlation in the postcue epoch]. Theta-gamma correlation of these 85 LFP pairs was based on 74 of 344 (21.5%) LFP channels contributing theta phases, and 67 of 344 (19.5%) LFPs contributing gamma-amplitude variations. Overall, 122 of 344 (35.5%) unique LFPs contributed to LFP pairs with theta-gamma correlation that was significant and consistently evident in both monkeys (*SI Result S1.1*). Observing reliable theta-gamma correlation was not dependent on the metric used to measure P-A correlation, as we found essentially identical results when we applied the weighted phase-locking factor (15) (Fig. S4). Consistent with this finding, we observed in 73% of those LFPs that provided the theta phase for significantly P-A-correlated pairs an apparent theta-band peak in the power spectra (Figs. S5 and S6). Power modulations at theta did not, however, correlate with cue-triggered increases of theta-gamma correlations (*SI Result S4*).

We next tested whether the LFP gamma-amplitude variations were statistically more precisely locked to the theta phases of LFPs or to the cue onset. If the latter were the case, then theta-gamma correlations could be secondary to cue-triggered gamma-amplitude changes (10). However, we found on average across

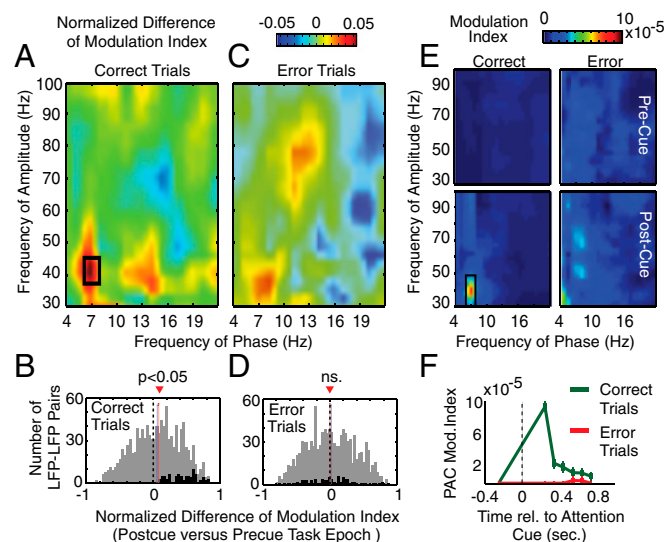


Fig. 2. Theta-gamma correlation is significantly enhanced after attention cue onset on correct trials. (A) Comodulograms of the normalized difference in the phase (x axis)-to-amplitude (y axis) correlation (measured as MI) in the postcue relative to the precue task epoch on correct trials ($n = 1,104$). Positive values indicate increases of P-A correlation after attention cue onset. The black rectangle denotes significant ($P < 0.05$) comodulation difference. (B) Histogram of the difference in theta-gamma P-A correlation MI in the postcue relative to precue task epoch across all LFP-LFP pairs on correct trials ($n = 1,104$). Black bars in both panels highlight those LFP pairs that exhibited an individually significant P-A correlation increase with attention on correct trials ($n = 85$). Red and blue vertical bars denote mean and median of the distribution, and the dotted line highlights the difference in MI of zero. (C and D) Same format as A and B but for error trials. Note that, in D, the black bars in the histogram show the theta-gamma MI values for the same LFP pairs highlighted in B. (E) Comodulograms showing the average P-A MI on correct trials (left column) and error trials (right column), and in the precue task epoch (upper row) and the postcue epoch (bottom row) ($n = 85$). Shown are the average MIs of those LFP-LFP pairs with significantly increased theta-to-gamma P-A correlation (the black-colored bars in B). (F) Temporal evolution of theta-gamma P-A correlation for those LFP pairs with a significant P-A correlation effect on correct trials ($n = 85$) during correct (green) and error (red) trials at different 500-ms time windows relative to the attention cue onset (x axis).

the $n = 85$ LFP pairs with significant theta–gamma correlations that the maximum gamma amplitudes showed less variance in the phase of their theta-band modulation than in their time to attention cue onset (*SI Result S5*; Fig. S3C).

Theta–Gamma Correlations Fail to Emerge on Error Trials. Theta–gamma P–A correlations could accompany attention cues irrespective of whether attention shifted correctly, which would render the phenomenon functionally unimportant. We thus compared correctly performed trials to error trials, where subjects either responded to the distractor (indicating either wrong attention shifts or low attentional control levels) or made wrong choices to the target (indicating, e.g., failed perceptual discrimination of the attended stimulus likely also related to low attentional control levels) (2, 16). In contrast to correct trials, the attention cue did not trigger a significant increase in P–A correlation on error trials (Wilcoxon sign-rank test, $P = 1$, FDR corrected; Fig. 2C). The lack of P–A correlation was evident across the whole population of LFP pairs as well as for the subset of LFP pairs that showed individually significant P–A correlation on correct trials (Fig. 2D). This functional effect is readily visible in the average MI comodulograms (Fig. 2E) and remained robust when equalizing the number of correct trials to the lower number of error trials (*SI Result S6*). Testing the temporal specificity of this error-predicting effect across all LFP pairs showed that theta–gamma correlations were maximal on correct trials immediately following cue onset, but remained higher than chance levels, and higher than on error trials, over the entire postcue analysis period (up to 0.75 ± 0.25 s) (Fig. 2F).

The lack of P–A correlations on error trials may follow from a larger variability of theta phases at which gamma activity synchronizes, from a systematic shift in theta-frequency locked phases, or a combination of both (17). To elucidate these possibilities, we characterized the theta phase at which gamma-activity modulations aligned on correct and on error trials (Fig. 3). Across LFP pairs with significant theta–gamma correlation, gamma bursts on correct trials phase locked on average close to the peak of the theta cycle after the attention cue (mean phase of -14.69° , 95% CI $[-41.01^\circ, 11.63^\circ]$), with a significantly non-uniform circular phase distribution (Hodges–Ajne test, $P = 3.6 \times 10^{-4}$; Fig. 3A). In contrast, the distribution of phases on error trials only revealed a statistical trend to deviate from uniformity (Hodges–Ajne test, $P = 0.064$), with a mean phase that was about 90° offset from the mean phase on correct trials (-94.28° , 95% CI $[-131.40^\circ, -57.16^\circ]$; Fig. 3B). Importantly, correct and error trial phase distributions were significantly different (Kuiper test, $P < 0.005$), suggesting that, on error trials, theta phases shifted and showed a larger variability compared with correct trials (Fig. 3C; see *SI Result S1.2* for consistent effect across monkeys). Control analyses revealed the same functional effects when we accounted for the lower overall modulation strength on error trials compared with correct trials (*SI Result S7*

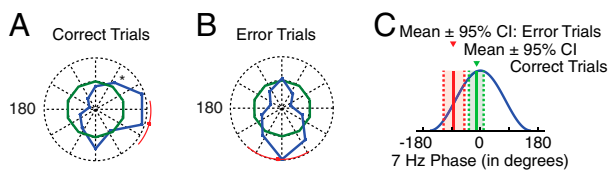


Fig. 3. Preferred theta phase of theta–gamma correlation on correct and error trials. (A) Polar histogram of the amplitude-weighted mean preferred phases in the postcue period at which gamma activity phase locked in those LFP pairs with significant theta–gamma coupling in the postcue period ($n = 85$). Colors denote the distributions expected by chance (green) and from the post-attention cue epoch (blue) on correct trials. The outer dotted ring corresponds to a proportion of 20%. The red dot and line denote circular mean and 95% confidence range. (B) Same as in A, but for error trials. (C) Illustration of the mean and 95% confidence range of the preferred theta phases on correct (green) and error trials (red) at which gamma amplitudes couple for the LFP pairs that showed a significant increase in theta–gamma P–A correlation after attention cue onset.

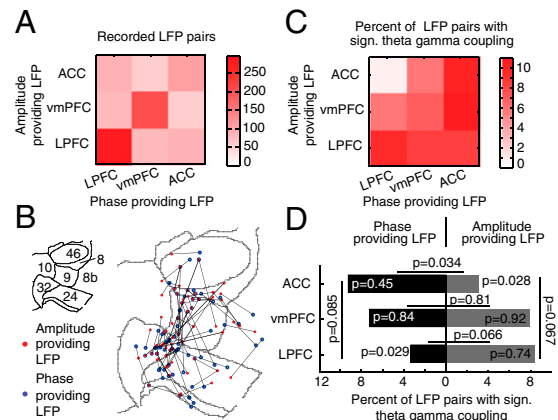


Fig. 4. Anatomical origins of cortical sites with phase and amplitude modulation during theta–gamma P–A correlation. (A) Combination matrix showing the total number of LFP–LFP pairs ($n = 1,104$) recorded from the ventromedial PFC (vmPFC) (areas 32 and 10), the anterior cingulate cortex (ACC) (area 24), and the LPFCs (areas 46, 8, and 9). The brain area of the phase-providing channels is on the x axis, and the origin of the amplitude-providing LFP channels is on the y axis. (B) Anatomical recording location of phase (blue) and amplitude (red) providing LFPs ($n = 85$ LFP pairs; connected with black lines) and plotted on the 2D flat-map representation of the ACC and PFC. Gray contours denote area boundaries (see *Inset* for area labels; Fig. 1B). (C) Same as in A, but for the proportion of theta–gamma P–A-correlated LFP pairs ($n = 85$) relative to all LFP pairs recorded for an area combination. Color indexes the proportion. (D) Likelihood to find a phase-providing channel (values *Left* from zero) and an amplitude-providing channel (*Right* from zero) in the vmPFC, ACC, and LPFC during cross-area theta–gamma correlation ($n = 32$; y axis).

and Table S1), as well as for the differences in trial numbers (*SI Result S6*). Moreover, we found that the average field potential of the LFP around the attention cue onset did not distinguish correct from error trials, suggesting that possible nonstationary transients do not account for the functionally significant P–A correlations (10) (*SI Result S8*).

Interareal Cross-Frequency Correlation Is Anatomically Specific. We next asked whether the anatomical location of the theta-phase- and gamma- amplitude-providing LFPs in ACC/PFC mattered for P–A correlations. One assumption of this analysis is that theta-phase-providing sites may more likely serve as modulating sources for attention, whereas gamma-amplitude-providing sites relate to implementing attention. To test this, we reconstructed the LFP recording locations (Fig. S1) and grouped them into the ventromedial PFC (vmPFC) (areas 32 and 10), ACC (area 24), and LPFC (areas 46, 8, and 9) (Fig. 4A). We found that, among the significantly theta–gamma correlated pairs, phase- and amplitude-providing LFPs were found in each of the subareas, but with an apparent asymmetry between areas (Fig. 4B and C; *SI Result S9* and *SI Result S1.3*). Testing each area for whether they contained more phase or amplitude LFPs, we found that LPFC theta phases were significantly less likely to correlate with ACC gamma amplitudes (Z test, $P = 0.0089$; Fig. 4C). More specific testing of the interareal P–A correlations showed that the LPFC had overall less interareal theta-phase-providing LFPs than expected by chance (Z test, $P = 0.029$; Fig. 4D), whereas the ACC had less interareal amplitude-providing LFPs (Z test, $P = 0.028$; Fig. 4D). Consistent with this finding, the ACC provided overall significantly more theta-phase LFPs than gamma-amplitude LFPs during interareal theta–gamma correlations (McNemar χ^2 test, $P = 0.034$; Fig. 4D), whereas the LPFC showed a trend for more amplitude- than phase-providing LFPs (McNemar χ^2 test, $P = 0.066$; Fig. 4D). These results were similar in both monkeys (*SI Result S1.3*).

Cue Induced Theta-Phase Reset in LFPs Showing Theta–Gamma Correlation. Theoretical studies suggest that the modulation of low-frequency phase is instrumental in triggering high-frequency

bursts during theta–gamma correlations (17, 18). Such precedence of low-frequency activity for P–A correlation would empirically become evident as a realignment, or reset, of phases (19). We tested for the presence of an attention cue-triggered theta-phase reset and its putative relation to theta–gamma correlation, and found that immediately following the attention cue the average theta-band phases became highly similar across individual LFPs that showed significant theta–gamma correlations. This phase alignment was visually apparent on correct trials but not on error trials (Fig. 5A). To quantify this phase reset, we calculated the significance of the instantaneous theta-phase consistency across trials for each LFP around attention cue onset and found that the greatest number of LFP channels exhibited significant theta-phase consistency 268 ms after attention cue onset (Fig. 5B, *Left*). The rise in theta-phase-consistent LFPs was evident on correct trials and failed to emerge on error trials. To validate this finding, we extracted the time at which the Rayleigh Z time course peaked in the 1,000 ms around the time of the attention cue onset for each LFP. Corroborating the previous result, we found that 41.89% of the theta-phase-providing LFP sites (31 of 74) showed peak phase consistency 150–250 ms (± 50 ms) after attention cue onset on correct trials (Fig. 5B, *Right*). This distribution of peak phase consistency was significantly non-uniform on correct trials, but not on error trials (Pearson's χ^2 test, $P = 0.0012$ and $P = 0.465$, respectively). In the 150- to 250-ms (± 50 -ms) time window, 35 of 74 LFP sites showed a significant theta-band phase consistency, and clustered at the nexus of the ACC, vmPFC, and LPFC (Fig. 5C).

The presence of a theta-phase reset could synchronize LFP theta phases across multiple ACC/PFC subfields. Thus, the correlation of gamma amplitudes to theta phases could be understood as a direct consequence of such large-scale theta-band coherence. However, we found that LFP–LFP theta-phase synchronization did not change from pre- to post-attention cue, was not different between correct and error trials, and did not correlate with the increase of interareal theta–gamma correlation during attention shifts (*SI Result S10*).

Selective Theta–Gamma Correlation for Target Locations and Its Relation to Firing-Rate Information. Theta–gamma correlation may not only emerge selectively on correct vs. erroneous attention shifts but may carry specific task-relevant information about direction of the attention shift. Across the entire population of LFP pairs, we found a statistical trend for larger theta–gamma correlation when attention shifted to the contralateral vs. ipsilateral stimulus (Wilcoxon sign-rank test, $P = 0.066$; Fig. S7A and *SI Result S11.1*). Testing for significant differences in theta–gamma correlation between spatial conditions at the single LFP pair level revealed that a small subset of LFP pairs (4.4%; 49 of 1,104) showed significant effects (Monte Carlo surrogate test, two-sided, $P < 0.05$), with $n = 32$ ($n = 17$) LFP pairs showing larger theta–gamma correlations for contralateral (ipsilateral) attention shifts (*SI Result S11.1*). This spatially selective theta–gamma correlation may relate to previously reported spatially selective firing-rate modulations of neurons in ACC/PFC (3, 20). However, we found that spatial selectivity in theta–gamma correlations were not consistently related to spatially selective firing of neurons recorded from the LFP recording sites that provided theta-phase or gamma-amplitude variations underlying theta–gamma correlations (all $r < 0.1$, $P > 0.05$; *SI Result S12*). In addition to spatial attention, we tested in a subset of sessions whether theta–gamma correlations emerged differentially when the cue directed attention to a target stimulus with higher vs. lower reward association, but did not find consistent differences of theta–gamma correlations for higher or lower rewarded attention targets (*SI Result S11.2*). Theta–gamma correlations for location or reward were largely unrelated to LFP pairs with theta–gamma correlations predictive of correct choices (Fig. S7B and *SI Result S11.1* and *SI Result S11.2*).

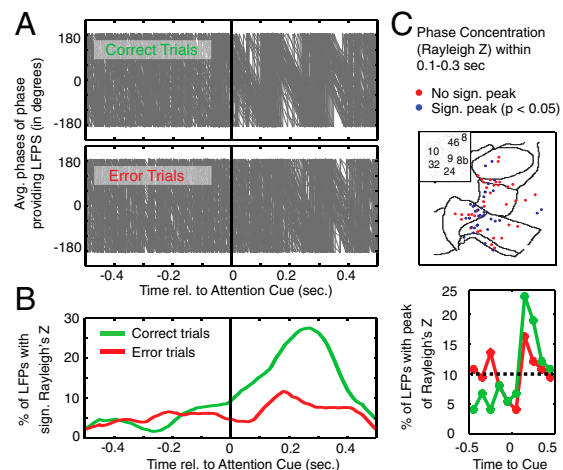


Fig. 5. Phase-providing LFPs engaging in significant theta–gamma phase-amplitude correlation show a theta-phase reset after attention cue onset on correct trials. (A) Progression of the average phase (y axis) for all phase-providing LFP channels ($n = 74$) engaging in significant theta–gamma correlation around the time of the attention cue onset (x axis). Each gray line represents the average phase across trials of one such LFP. Top and bottom panels show the progression of mean phases on correct trials and on error trials, respectively. (B) The left panel shows the percentage of phase-providing channels with significant phase concentration (y axis, measured as Rayleigh's Z) around the time of the attention cue onset (x axis). Green and red lines show the average Rayleigh's Z across LFP channels for correct and for error trials, respectively. The panel on the *Right* shows the percentage of LFPs whose peak phase concentration fell within 1 of 10 nonoverlapping time bins (around attention cue onset). (C) The anatomical distribution of recorded LFPs that showed a significant phase concentration (blue) or that did not show significant phase concentration (red) in the 0.1–0.3 s following attention cue onset. See Fig. 1B for the labeling of PFC/ACC brain areas on the 2D flat-map representation (and Figs. 1 and 2).

Theta–Gamma Correlation and Its Relation to Synchronization of Burst Firing Events. Although overall firing-rate modulations of neurons were not statistically associated with theta–gamma correlations (*SI Result S12*), it is possible that finer-grained burst firing events relate to long-range theta–gamma correlations, similar to burst firing events synchronizing long-range to mid-gamma-band (55–75 Hz) LFP activity (12). We thus correlated burst–LFP synchronization of neurons recorded at LFP recording sites that provided theta-phase or gamma-amplitude variations for theta–gamma correlations (*SI Result S13*). We found that burst synchronization to remote LFP gamma activity varied proportionally with the degree of theta-phase correlation with low-gamma amplitudes (35–50 Hz), an effect that was limited to those LFP sites that showed significant theta–gamma correlations (Spearman rank correlation $r = 0.2$, $P = 0.044$; Table S2 and *SI Result S13*). To our knowledge, these findings provide the first quantitative evidence that recording sites with LFP theta phases that engage in long-range gamma correlations also host neurons whose burst firing events synchronize long-range to gamma activity.

Discussion

We found that a centrally presented attention cue induces a correlation of 5–10 Hz theta-band phase fluctuations and 35–55 Hz gamma-band activations between cortical subfields in ACC/PFC. This theta–gamma P–A correlation failed to increase on erroneous trials and thus signified successful shifts of attention, i.e., cue utilization. On error trials, preferred theta phases were earlier and more variable in the theta cycle compared with correct trials. This suggests that failures of shifting attention are associated with the decoherence of theta to gamma interactions in a network comprising the ACC/PFC. In this network, the theta–gamma P–A correlations were supported disproportionately often by theta phases from within the ACC compared with the

LPFC. This finding indicates that it is particularly the ACC (the rostral part of area 24) that provides a critical, slow theta-periodic influence on gamma-mediated processes within the LPFC during the implementation of attention shifts. A further major characteristic of theta–gamma correlation is its close association with a cue-induced theta-phase reset. More than one-third of phase-providing LFPs for significant theta–gamma P–A correlation showed the largest theta-phase consistency within the first 0.3 s following cue onset, suggesting that a theta-phase reset could mechanistically be a source of anatomically widespread theta–gamma correlation. Taken together, these findings provide a unique perspective on how the control of attention is implemented by circuits in primate ACC/PFC and corroborate a long-held hypothesis that theta–gamma cross-frequency interactions are an essential means of interareal integration of distributed activities in multinode cortical networks (9, 21).

Frequency Specificity of P–A Correlation in ACC/PFC. Our main finding characterized the statistical relation of two band-limited activity fluctuations comprising a narrow ~5- to 10-Hz (peak at 7 Hz) theta band and a ~35- to 55-Hz (peak at 40 Hz) gamma band. Previous studies have documented that a 5- to 10-Hz theta band is a widespread LFP signature in ACC/PFC that increases with specific demands to control goal-directed behavior (22–25). Our study corroborates these reports (Fig. S5) revealing that theta-band activity synchronizes distributed bursts of gamma activity in ACC/PFC to preferred phases of the theta oscillation. This further supports the notion that theta–gamma P–A correlation is a ubiquitous phenomenon evident across multiple circuits including hippocampal-cortical circuits (26), hippocampal-striatal networks (27), cortico-striatal networks (28), and cortico-cortical networks (29, 30). Our results extend the role of theta–gamma P–A correlation to PFC circuits, with ~35% of LFP sites contributing to significant theta–gamma interactions. However, these sites show anatomically specific clustering, with a moderate maximal ~8–10% of interareal ACC–theta to LPFC–gamma pairs showing individually significant effects (Fig. 4).

In previous studies, 5- to 10-Hz activity fluctuations were shown to organize distinct band-limited gamma-frequency bands categorized as low (~35–55 Hz), medium (~50–90 Hz), and high (epsilon; ~90–140 Hz) bands, each likely originating in separable underlying circuit motifs (8, 11, 26). The observation that ACC/PFC circuits theta-synchronized the activation at a low-gamma-frequency band (35–55 Hz) is, to our knowledge, unprecedented in LFP recordings in the primate brain. However, a similar theta to low-gamma P–A correlation has been found in rodents to emerge in medial frontal, entorhinal, and hippocampal circuits (8, 26, 27, 31). In the cortex of nonhuman primates, synchronization of a low (35–55 Hz) gamma-frequency band has recently been described to characterize local LFP and spike–LFP coherence within the macaque frontal eye field (FEF) during sustained selective attention (32) (for a lower 30- to 40-Hz beta/gamma in LPFC, see ref. 33). The cortical ACC/PFC fields engaging in theta-locked low-gamma activation in our study anatomically connect to the FEF. This makes it likely that the theta-phase reset we observed in ACC/PFC also synchronizes FEF gamma-activity bursts and spiking activity of visually selective FEF neurons that most strongly synchronize to the local, low-gamma activity in FEF during sustained selective attentional processing (34). We can thus speculate that the band-limited neuronal activation of the specific theta and gamma bands that interact during attention shifts in our study may serve as general band-limited signatures of neuronal coordination of attention information during goal-directed behaviors.

Functional Significance of Theta-Phase Resets in the ACC/PFC. The attention cue-triggered P–A correlations we observed were associated with a prominent theta-phase reset. Similar to the absence of theta–gamma P–A correlation on error trials, the theta phase failed to reset following the attention cue on error trials (Fig. 5B), illustrating that the LFP theta-phase resets of the

theta-gamma-correlated network also indexed whether attention shifts are successful. A plausible mechanism for such a far-reaching consequence of phase-aligned theta activation can be found in recent studies that identified how a cue-induced phase reset effectively gates the outflow of a cortical circuit (35–37). These studies suggest that the phase reset-gated output of a local circuit can serve as the causal trigger of distant gamma activity phase locked to theta activity. For example, one optogenetic study documented that a locally generated theta-phase reset in rodent frontal cortices develops in conjunction with learning the meaning of a (classically conditioned) cue (37). Following learning, the cue-triggered theta-phase reset predicted when projection neurons phase lock their spike output to the peak of theta oscillation cycles (37). Moreover, the theta-phase reset effectively synchronized the spiking activity of those projection neurons in rodent mPFC that activated fear-related target structures that modified behavior. The attention cue-induced phase reset we report may be analogous to such a sequence of events. In our task, the cue signified a color-matching rule (“find the peripheral stimulus matching the color of the cue and enhance its representation against other stimuli”). Correctly interpreting the cue required reactivating neural assemblies coding for the rule representation and applying the rule to the visually available information to eventually prioritize processing of the attended stimulus and filter out uncued stimuli (3, 38) (Fig. S8A). Such an attentional remapping of functional connectivity occurred in the first 0.5 s following attention cue onset (3), and it is during this process that theta phases were most consistent across trials and began to synchronize remote gamma activities across ACC/PFC. We therefore speculate that the cue-triggered theta reset is instrumental to synchronize ACC/PFC neural circuits to theta rhythmic, ~140-ms-long activation periods that provide a reference for phase-locked gamma-activity bursts.

Three additional sources of evidence support this prediction and are in line with our results. First, studies in rodents suggest that theta-phase resets and theta coupling to gamma emerges in a prefrontal–hippocampal network to widely varying types of instructional cues, ranging from (Pavlovian) cues in classical conditioning contexts (31, 37), to instrumental cues in spatial choice tasks and item-context association tasks (27, 39). Second, computational studies have identified canonical circuit motifs of theta–gamma correlation in which the theta phase can be instrumental in triggering and even generating gamma-band activities in postsynaptic target circuits (17, 40). Key assumptions of such “theta-reset models” are the existence of a robust gamma-generating feedback circuit in the target structure, and a low-frequency (theta periodic)–modulated input to inhibitory cells in the circuit (17, 41, 42). This low-frequency (theta)–modulated input may likewise be generated de novo from within the circuit from theta-generating or theta-resonating interneuron populations (figure 1A in ref. 11; see Fig. S8 for other dynamic circuit motifs). Third, a large set of studies have documented how attentional expectancies realign phases of low frequencies in sensory cortices to the time when attentionally relevant stimuli are expected to occur to support goal-directed behavior (19). Such anticipatory phase entrainment resembles “resets” and can synchronize high-frequency activities at beta and gamma bands that correlate with sensory detection speed and the efficiency of subjects to filter out distractors in attention tasks (19, 43). Consistent with these findings, we found that, in a situation without externally imposed entrainment of events, attention cues induce a rapid phase reset and thereby possibly implement a covert selection of relevant sensory stimuli according to the cue-dependent instructional rule.

Theta–Gamma Correlation as Means to Coordinate Attention Information.

It is important to acknowledge that we found the theta-phase reset and theta–gamma P–A correlation in precisely those cortical circuits of the ACC/PFC that are functionally essential for the flexible control and biasing of attention- and goal-directed

behavior (1, 6). To realize such a control/bias function, ACC/PFC likely continuously interact with fronto-parietal attention networks during goal-directed behavior to ensure continued attention to relevant information that relate to the task goals and other working memory contents (1, 2). We believe that such biasing during attentive processes is realized through theta–gamma cross-frequency interactions involving circuits in ACC/PFC.

An important piece of information supporting the proposed “P–A correlation hypothesis of attentional control” is that burst spiking events related to theta–(low) gamma correlation. We found that burst firing of neurons synchronized to remote (mid) gamma-band activity at those LFP recording channels that provided the theta phases for LFP pairs with significant theta–gamma correlation. This result links findings on interareal burst synchronization (12) with the current report of functionally relevant theta–gamma correlations and suggests that interareal theta–gamma interactions of different LFPs may directly or indirectly relate to burst firing of neurons within the theta-frequency–modulated circuits. Intriguingly, firing of bursts or firing of sequences during brief periods of theta-nested gamma-band activity is strongly implicated in rodent hippocampus and striatum to carry unique information about internally maintained goals

(e.g., the location of the most rewarded outcome) (44, 45). Our results suggest that theta-nested gamma modulations may serve as a means to organize and integrate such covertly (internally) generated information to ensure the flexible control of attention during goal-directed behaviors.

Methods

Two macaque monkeys were trained on a selective attention task that required using a centrally presented color cue to covertly select (i.e., in the absence of overt eye movements) a color matching peripheral stimulus and ignore the nonmatching stimulus (Fig. 1A). During attention performance, we recorded LFPs from microelectrodes in anatomically reconstructed locations in the medial and lateral PFC (Fig. 1B). The full task is detailed in Fig. 1A and B and [Supporting Information](#). The experiment followed the guidelines of the Canadian Council of Animal Care policy on the use of laboratory animals and was approved by University of Western Ontario Council on Animal Care.

ACKNOWLEDGMENTS. We thank Dr. Daniel Kaping, Johanna Stucke, Iman Janemi, and Michelle Bale for help with the electrophysiological recordings and reconstruction of recording sites. This research was supported by grants from the Canadian Institutes of Health Research, the Natural Sciences and Engineering Research Council of Canada, and the Ontario Ministry of Economic Development and Innovation.

- Miller EK, Buschman TJ (2013) Cortical circuits for the control of attention. *Curr Opin Neurobiol* 23(2):216–222.
- Shenhav A, Botvinick MM, Cohen JD (2013) The expected value of control: An integrative theory of anterior cingulate cortex function. *Neuron* 79(2):217–240.
- Kaping D, Vinck M, Hutchison RM, Everling S, Womelsdorf T (2011) Specific contributions of ventromedial, anterior cingulate, and lateral prefrontal cortex for attentional selection and stimulus valuation. *PLoS Biol* 9(12):e1001224.
- Rushworth MF, Noonan MP, Boorman ED, Walton ME, Behrens TE (2011) Frontal cortex and reward-guided learning and decision-making. *Neuron* 70(6):1054–1069.
- Gläscher J, et al. (2012) Lesion mapping of cognitive control and value-based decision making in the prefrontal cortex. *Proc Natl Acad Sci USA* 109(36):14681–14686.
- Passingham RE, Wise SP (2012) *The Neurobiology of the Prefrontal Cortex: Anatomy, Evolution, and the Origin of Insight* (Oxford Univ Press, Oxford).
- Sirota A, et al. (2008) Entrainment of neocortical neurons and gamma oscillations by the hippocampal theta rhythm. *Neuron* 60(4):683–697.
- Belluscio MA, Mizuseki K, Schmidt R, Kempter R, Buzsáki G (2012) Cross-frequency phase–phase coupling between theta and gamma oscillations in the hippocampus. *J Neurosci* 32(2):423–435.
- Lisman JE, Jensen O (2013) The θ - γ neural code. *Neuron* 77(6):1002–1016.
- Aru J, et al. (2015) Untangling cross-frequency coupling in neuroscience. *Curr Opin Neurobiol* 31:51–61.
- Womelsdorf T, Valiante TA, Sahin NT, Miller KJ, Tiesinga P (2014) Dynamic circuit motifs underlying rhythmic gain control, gating and integration. *Nat Neurosci* 17(8):1031–1039.
- Womelsdorf T, Ardid S, Everling S, Valiante TA (2014) Burst firing synchronizes prefrontal and anterior cingulate cortex during attentional control. *Curr Biol* 24(22):2613–2621.
- Ardid S, et al. (2015) Mapping of functionally characterized cell classes onto canonical circuit operations in primate prefrontal cortex. *J Neurosci* 35(7):2975–2991.
- Tort AB, Komorowski R, Eichenbaum H, Kopell N (2010) Measuring phase-amplitude coupling between neuronal oscillations of different frequencies. *J Neurophysiol* 104(2):1195–1210.
- van Wingerden M, van der Meij R, Kalenscher T, Maris E, Pennartz CM (2014) Phase-amplitude coupling in rat orbitofrontal cortex discriminates between correct and incorrect decisions during associative learning. *J Neurosci* 34(2):493–505.
- Shen C, et al. (2014) Anterior cingulate cortex cells identify process-specific errors of attentional control prior to transient prefrontal-cingulate inhibition. *Cereb Cortex*, 10.1093/cercor/bhu028.
- Onslow AC, Jones MW, Bogacz R (2014) A canonical circuit for generating phase-amplitude coupling. *PLoS One* 9(8):e102591.
- Zhang X, Kendrick KM, Zhou H, Zhan Y, Feng J (2012) A computational study on altered theta-gamma coupling during learning and phase coding. *PLoS One* 7(6):e36472.
- van Atteveldt N, Murray MM, Thut G, Schroeder CE (2014) Multisensory integration: Flexible use of general operations. *Neuron* 81(6):1240–1253.
- Tremblay S, Pieper F, Sachs A, Martinez-Trujillo J (2015) Attentional filtering of visual information by neuronal ensembles in the primate lateral prefrontal cortex. *Neuron* 85(1):202–215.
- McGinn RJ, Valiante TA (2014) Phase-amplitude coupling and interlaminar synchrony are correlated in human neocortex. *J Neurosci* 34(48):15923–15930.
- Tsujimoto T, Shimazu H, Isomura Y, Sasaki K (2010) Theta oscillations in primate prefrontal and anterior cingulate cortices in forewarned reaction time tasks. *J Neurophysiol* 103(2):827–843.
- Womelsdorf T, Johnston K, Vinck M, Everling S (2010) Theta-activity in anterior cingulate cortex predicts task rules and their adjustments following errors. *Proc Natl Acad Sci USA* 107(11):5248–5253.
- Liebe S, Hoerzer GM, Logothetis NK, Rainer G (2012) Theta coupling between V4 and prefrontal cortex predicts visual short-term memory performance. *Nat Neurosci* 15(3):456–462, S451–S452.
- Phillips JM, Vinck M, Everling S, Womelsdorf T (2014) A long-range fronto-parietal 5- to 10-Hz network predicts “top-down” controlled guidance in a task-switch paradigm. *Cereb Cortex* 24(8):1996–2008.
- Colgin LL, et al. (2009) Frequency of gamma oscillations routes flow of information in the hippocampus. *Nature* 462(7271):353–357.
- Tort AB, et al. (2008) Dynamic cross-frequency couplings of local field potential oscillations in rat striatum and hippocampus during performance of a T-maze task. *Proc Natl Acad Sci USA* 105(51):20517–20522.
- von Nicolai C, et al. (2014) Corticostriatal coordination through coherent phase-amplitude coupling. *J Neurosci* 34(17):5938–5948.
- Canolty RT, et al. (2010) Oscillatory phase coupling coordinates anatomically dispersed functional cell assemblies. *Proc Natl Acad Sci USA* 107(40):17356–17361.
- Bosman CA, et al. (2012) Attentional stimulus selection through selective synchronization between monkey visual areas. *Neuron* 75(5):875–888.
- Shearkhani O, Takehara-Nishiuchi K (2013) Coupling of prefrontal gamma amplitude and theta phase is strengthened in trace eyeblink conditioning. *Neurobiol Learn Mem* 100:117–126.
- Gregoriou GG, Gotts SJ, Zhou H, Desimone R (2009) High-frequency, long-range coupling between prefrontal and visual cortex during attention. *Science* 324(5931):1207–1210.
- Siegel M, Warden MR, Miller EK (2009) Phase-dependent neuronal coding of objects in short-term memory. *Proc Natl Acad Sci USA* 106(50):21341–21346.
- Gregoriou GG, Gotts SJ, Desimone R (2012) Cell-type-specific synchronization of neural activity in FEF with V4 during attention. *Neuron* 73(3):581–594.
- Rizzuto DS, et al. (2003) Reset of human neocortical oscillations during a working memory task. *Proc Natl Acad Sci USA* 100(13):7931–7936.
- McCartney H, Johnson AD, Weil ZM, Givens B (2004) Theta reset produces optimal conditions for long-term potentiation. *Hippocampus* 14(6):684–687.
- Courtin J, et al. (2014) Prefrontal parvalbumin interneurons shape neuronal activity to drive fear expression. *Nature* 505(7481):92–96.
- Buschman TJ, Denovellis EL, Diogo C, Bullock D, Miller EK (2012) Synchronous oscillatory neural ensembles for rules in the prefrontal cortex. *Neuron* 76(4):838–846.
- Benchenane K, et al. (2010) Coherent theta oscillations and reorganization of spike timing in the hippocampal–prefrontal network upon learning. *Neuron* 66(6):921–936.
- Neymotin SA, et al. (2013) Ih tunes theta/gamma oscillations and cross-frequency coupling in an in silico CA3 model. *PLoS One* 8(10):e76285.
- Wulff P, et al. (2009) Hippocampal theta rhythm and its coupling with gamma oscillations require fast inhibition onto parvalbumin-positive interneurons. *Proc Natl Acad Sci USA* 106(9):3561–3566.
- Pastoll H, Solanka L, van Rossum MC, Nolan MF (2013) Feedback inhibition enables θ -nested γ oscillations and grid firing fields. *Neuron* 77(1):141–154.
- Bonnefond M, Jensen O (2012) Alpha oscillations serve to protect working memory maintenance against anticipated distracters. *Curr Biol* 22(20):1969–1974.
- Gupta AS, van der Meer MA, Touretzky DS, Redish AD (2012) Segmentation of spatial experience by hippocampal θ sequences. *Nat Neurosci* 15(7):1032–1039.
- Pezzulo G, van der Meer MA, Lansink CS, Pennartz CM (2014) Internally generated sequences in learning and executing goal-directed behavior. *Trends Cogn Sci* 18(12):647–657.
- Barbas H, Zikopoulos B (2007) The prefrontal cortex and flexible behavior. *Neuroscientist* 13(5):532–545.
- van der Meij R, Kahana M, Maris E (2012) Phase-amplitude coupling in human electrocorticography is spatially distributed and phase diverse. *J Neurosci* 32(1):111–123.
- Berens P (2009) CircStat: A MATLAB toolbox for circular statistics. *J Stat Softw* 31(10):1–21.
- Zar JH (2010) *Biostatistical Analysis* (Pearson Prentice-Hall, Upper Saddle River, NJ).
- Maris E, Oostenveld R (2007) Nonparametric statistical testing of EEG- and MEG-data. *J Neurosci Methods* 164(1):177–190.